Laboratory for Atmospheric and Space Physics

University of Colorado
Boulder, Colorado

National Aeronautics and Space Administration
Total and Spectral Solar Irradiance Sensor
(NASA TSIS-1)

Algorithm Theoretical Basis Document – Post Launch Update

Total Irradiance Monitor (TIM)

Document No. Draft Date: 29 Nov. 2020

Description/Summary/Contents:

In this document we present updates to the Level-1 processor algorithms used for the Total Irradiance Monitor (TIM) flying on the TSIS-1 platform to accommodate an alternate approach from that in the pre-launch ATBD that was reviewed and published June 2017. This ATBD applies to post-launch processing only.

Prepared by Greg Kopp Date Aug. 2020

Prepared by David Harber Date Aug. 2020

Prepared by Erik Richard Date Aug. 2020

Prepared by Brandon Stone Date Aug. 2020

Approved by _____ Date _____

Revisions				
Rev	Description of Change	By	Approved	Date

Outline

1 Introduction

1.1 Purpose of this Document

This supplemental Algorithm Theoretical Basis Document (ATBD) describes updates to the Level-2 processor algorithms used for the Total Irradiance Monitor (TIM) flying on the TSIS-1 platform to accommodate an alternate analysis approach from that in the pre-launch ATBD that was reviewed and published in June 2017 [1]. This document is a supplement to that full ATBD and does not attempt to redundantly replicate the descriptions in that document. This ATBD applies to post-launch data processing and a post-launch redetermination of the TIM non-equivalence calibrations.

1.2 Scope

In conjunction with the original TSIS-1/TIM ATBD [1], this document describes updates to those algorithms to generate more accurate TSI data sets from direct observations of the Sun from space. An analysis approach incorporating DC subtraction (DCS) instead of or in conjunction with phase-sensitive detection (PSD) is presented here. The focus is on the processing algorithm changes and the updates that have improved the TIM uncertainties incorporated beginning with V.3 Level-3 data, which were originally released in May 2020.

1.3 Applicable Documents

The initial TSIS-1 ATBD [1] remains the primary ATBD for this mission. This TIM-specific post-launch ATBD merely provides updates for TIM processing changes incorporated beginning with V.3 data.

1.4 Contributing Authors

Greg Kopp	TIM Instrument Scientist
David Harber	TSIS Calibration Lead
Erik Richard	SIM Instrument Scientist
Brandon Stone	TIM Data-Systems Processing Specialist

2 Overview and Background Information

2.1 TSIS-1 TSI Science Goals and Objectives

The science and mission goals are unchanged from those in the original TSIS-1 ATBD. The key goals relevant to this document are repeated here:

- Measure the total solar irradiance (TSI) four times daily with an absolute accuracy of 100 ppm (baseline), 350 ppm (threshold), and a relative accuracy of ±10 ppm and provide calibrated overlap with the SORCE/TIM, TCTE/TIM, and available future missions.

2.2 On-Orbit Progression of Stated TSIS-1/TIM Uncertainties

The initial (V.1 and V.2) TSIS-1/TIM TSI data releases reported time-dependent uncertainties of 450 ppm (k=1) that improved to 410 ppm with updates to instrument-applied proportional–integral–derivative (PID) coefficients on 9 April 2018. These uncertainties were largely due to cavity-to-cavity differences in the TSI values that were computed

from on-orbit observations using the PSD algorithms common to the SORCE, TCTE, and TSIS-1 TIM data-processing systems and described in the TSIS-1 ATBD [1]. Applying a more fundamentally straightforward DCS analysis reduced the cavity-to-cavity differences to 66 ppm (as of April 2020 with the analysis leading to V.3) and an updated uncertainty budget of approximately 114 ppm for the instrument's primary cavity. Using this DCS approach, which is based on a three-half-cycle (150-second total) Hanning filter function, however, increases the short-term noise in the TSI time series by > 2×.

The current TSIS-1/TIM TSI data version (V.3) is the third public data release and the first to use a hybrid-PSD analysis approach. This approach uses the DCS method to derive the non-equivalence value of each cavity needed to make the PSD- and DCS-computed values agree. These non-equivalence values are then implemented in the PSD-based measurement equation, maintaining the low-noise advantages and the heritage of that approach while benefitting from the accuracy of the DCS approach via the on-orbit-derived non-equivalence calibration values. The calibration updates in this release have improved the stated uncertainties from those in prior versions particularly in regard to the absolute-value uncertainties.

These V.3 data meet all mission threshold requirements. These TSI results and the estimated net time-dependent uncertainties and their contributions are described in §5.2 and §5.3, respectively.

3 Instrument Design

3.1 Overview

The TIM design is unchanged from that described in the original TSIS-1 ATBD [1] and is largely unchanged from the original SORCE/TIM instrument, a detailed description of the design and calibrations of which are given by Kopp *et al*. [3,4].

Fundamentally, the TIM is a four-channel, ambient-temperature electrical-substitution radiometer (ESR) with each physical ESR consisting of an absorptive cylindrical/conical cavity. These are pairwise thermally balanced. The four channels provide redundancy and allow for solar-exposure-dependent degradation tracking via duty cycling.

Each cavity, via its thermistor, forms a bolometer to detect incoming solar radiation, which is modulated by a digitally-controlled mechanical shutter operating at 0.01 Hz with a 50% opened/closed duty cycle. A digital AC feedback loop controls bolometer heating via a precision wire-wound resistor near the tip of the conical section of each cavity. The electronics consist of the difference-temperature sensing bridge, a bridge-error amplifier, precision voltage sources, and a DSP-implemented servo loop for actively balancing the bridge, as shown in Figure 1. The thermistor temperature sensors on each of the two bolometers form two legs of the bridge with the opposing load resistors set to 0.75 of the operating resistance of the thermistors. This bridge configuration stabilizes the bias heating power (aka "gain") against ambient temperature changes. Any differential bolometer temperature unbalances the bridge and the resulting error signal is amplified, digitized, demodulated, filtered via a PID-controlled servo system, and then fed back to the cavity heater at 100 Hz from a 16-bit pulse-width modulator digital-to-power converter. During normal operations a feed-forward matched to the anticipated solar power is applied concurrent with shutter transitions, thereby keeping the cavity temperature nearly constant as incident sunlight is modulated. Comparing the active bolometer cavity to a reference cavity that is shielded from sunlight eliminates sensitivity to common-mode thermal variations.

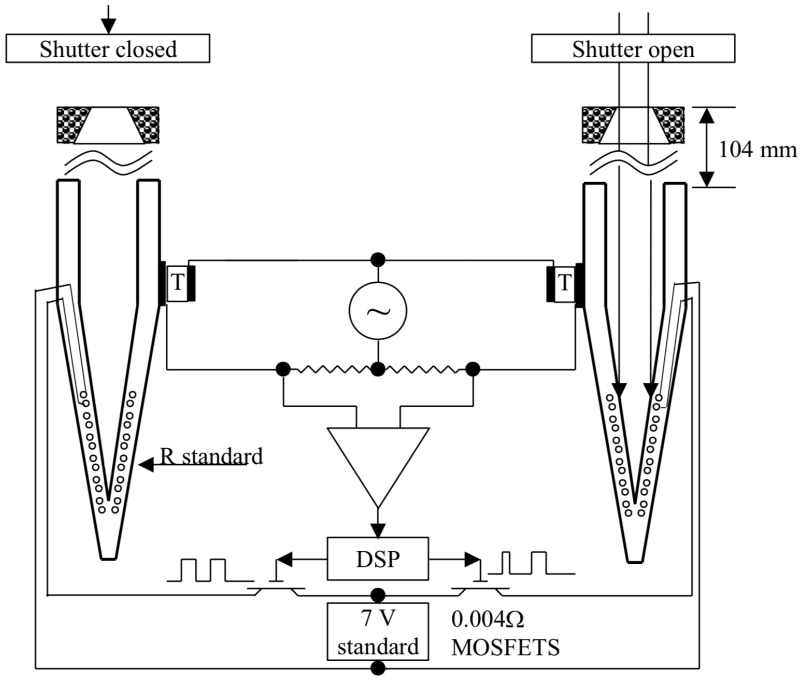

Figure 1: Schematic of the TIM servo system. Thermistors *T* on the cavities detect differential temperature changes. The DSP-controlled servo system adjusts the electrical heater power to the active cavity to keep the temperature constant as sunlight is modulated by a shutter. A precision DC reference voltage is pulse-width modulated through low resistance switches to the standard heater resistances on the cavities. The thermistor locations shown are the placements on the SORCE/TIM cavities. Those on the TSIS-1/TIM are located approximately halfway between those shown here and the foremost portion of the heater winding ('R_standard,' indicated by the small circular cross-sections).

One notable difference between the SORCE and TSIS-1 TIM instruments is the location of the cavities' high-resolution thermistors (*T* in Figure 1), which regulate the electrical bridge circuits. The TSIS-1 thermistors were moved closer to the precision wire-wound resistors near the tip of each cavity, increasing the bandwidth of the closed-loop control system. The location change was initially introduced, reviewed, and implemented for the Glory/TIM.

3.2 ELECTRICAL SUBSTITUTION RADIOMETER DETAILS

An abridged design explanation of the electrical-substitution radiometer (ESR) is reproduced here due to relevance in subsequent sections.

The TIM ESRs are thermally conductive cavities with high absorptivity across the entire solar spectrum. The high absorptivity ensures nearly all the entering sunlight is collected and converted into thermal energy within the cavity. This thermal energy is quickly transported to thermistors that monitor cavity temperature, so that the servo system maintaining the cavity temperature can respond quickly to changes in incident light. Electrical power is individually applied to each ESR cavity to maintain a constant temperature. A shutter in front of a precision aperture periodically opens, allowing incident sunlight to fall on the inside of the cavity behind that shutter. The increase in absorbed radiant energy is compensated by a measured reduction in electrical power to maintain constant cavity temperature. Conversely, when the shutter is closed again and no light is being absorbed by the ESR, increased electrical power must once again be supplied to maintain the same ESR temperature. This changing electrical power is "equivalent" to the changing incident radiant power, and thereby provides an accurate measure of that power.

The dominant path of the heat from the cavities to the heat sink is through stainless steel spokes that mechanically hold the cavities. The silver electrode spinel chip thermistors are soldered to each cavity near this support structure and sense relative changes (i.e. the thermistors require high resolution but not high absolute accuracy) from a nominal temperature in order to control the feedback loop for electrical-substitution heater power. The thermistors have a -4 %/°C Temperature Coefficient of Resistance (TCR). The thermal time constant of the cavities to the heat sink is approximately 220 seconds. All four ESR cavities are cantilevered from a central hub, ensuring that the active and reference cavities have the same thermal source (see Figure 1). Gold plating on the exterior surfaces of the cavities and heat sink reduces radiative coupling between the ESRs and their surroundings.

3.3 EQUIVALENCE-RATIO DETAILS

A description of the equivalence ratio is reproduced here due to relevance in subsequent sections.

The ESR heater power is supplied by a precision wire resistor wound around the conical section of the cavity to roughly match the region of solar illumination. The change in electrical power that gives precisely the same cavity temperature as that provided by the incident light is a measure of radiant power incident on the ESR cavity. In the construction of the heater, an attempt is made to match the distribution of heater power and incident radiant solar power. If the electrical power were applied with the same distribution as the absorbed radiation, the electrical and radiant powers would be exactly equivalent. The relationship between the distribution of electrical heater power and absorbed radiant power, referred to as the *equivalence ratio*, has both an AC and a DC component.

- **DC Non-Equivalence**: The DC component of the equivalence ratio is due to static heat differences in thermal heat flow for electrical and radiant power. The magnitude of the DC equivalence ratio can be determined through end-to-end measurements, such as those performed in the TSI Radiometer Facility (TRF) [5], and through detailed modeling of the heat flow through a cavity. *This value, often assumed to be unity, is needed for both the DCS and PSD analysis approaches.*
- **AC Non-Equivalence**: The AC component is not unity because of delay differences in conducting electrically-applied and radiant power (heat) from the rear of the cavity to the central thermistors. The non-equivalence effects are reduced by making the walls of the cavities thicker for reduced thermal impedances, matching the electrical-heater distribution (from the wire-wound resistor) to the radiation distribution (from incident sunlight), and increasing the thermal diffusivity of the cavity (thus the material selection of silver). The differential delays can be characterized by response measurements as a function of shutter frequency. *This value is needed only at the shutter frequency for the PSD method.*

The thermal response measured by the thermistors due to power applied to the electrical heater is characterized by the heater thermal impedance, Z_H. This transfer function, expressed here as a phasor, characterizes the magnitude and phase shift of the thermal response to electrically-applied power as a function of frequency. Likewise, the radiant-power thermal impedance, Z_R, is defined in a similar manner for radiant heating. The equivalence ratio is defined as the ratio of these two thermal impedances, Z_H/Z_R, and would be unity for an ideal ESR. However, due to delays in thermal propagation of the input electrical and radiant power, this term generally differs from unity, particularly at higher frequencies. Differences in the static heat flow or radiative losses between electrical and radiant heating may also cause this ratio to deviate from unity at DC.

The TIM cavity was specifically designed to collocate the heater and radiant power inputs at the back of the cavity in order to ensure an equivalence ratio very close to unity [3]. Initial analytical calculations of the non-equivalence ratio for the SORCE/TIM were $1.000008 + 0.0083i$ at the 0.01 Hz shutter fundamental.

During typical on-orbit operation, a feedforward is applied at the same time as a shutter transition so that when the shutter is opened the cavity heater power is reduced by an amount equal to the anticipated incoming radiant power. If

the equivalence ratio at all frequencies were unity and this feedforward matched the radiant incident power, no heater-response transient would be observed. Conversely, *any transient observed contains information about the equivalence ratio*.

During on-orbit operations of the SORCE/TIM, a larger transient than anticipated was observed. Frequency analysis of this transient (assuming that the equivalence ratio was unity at DC) gave an equivalence ratio at 0.01 Hz of 1.000215 + 0.004353*i*, causing a difference of 193 ppm in TSI from the value determined using the analytical calculation. This discrepancy between the analytical calculation and the measured AC component of the equivalence ratio illustrates that this ratio is difficult to estimate, and thus needs to be determined (or at least verified) using on-orbit measurements.

During the Glory/TIM instrument TRF measurements, Cavity A was illuminated with uniform irradiance, the instrument was shuttered, and a feedforward was applied. A larger transient than that for the SORCE/TIM was observed, and the resulting equivalence ratio at 0.01 Hz was measured to be 1.0008158 + 0.01394*i*. The cause of this larger non-equivalence was attributed to the reduced physical separation between the cavity heater and thermistors. With a significantly shorter distance to flow, small time differences between electrical and radiant inputs flowing to the thermistors create a larger relative difference, or a larger non-equivalence.

Earlier data versions (V.1 and V.2) of the TSIS-1/TIM assumed that the equivalence ratio at 0.01 Hz would be the same as that measured for the Glory/TIM (1.0008158 + 0.01394*i*) since the cavity designs are identical. However, on-orbit measurements indicate that this value differs for each cavity, as the responses to transients from each cavity differ (see Figure 2). These differences in the equivalence ratio for each cavity are likely due to small differences in the construction of each and are brought out in the TSIS-1/TIM more so than in prior spaceflight TIMs because of the cavity thermistor placement described in §3.1.

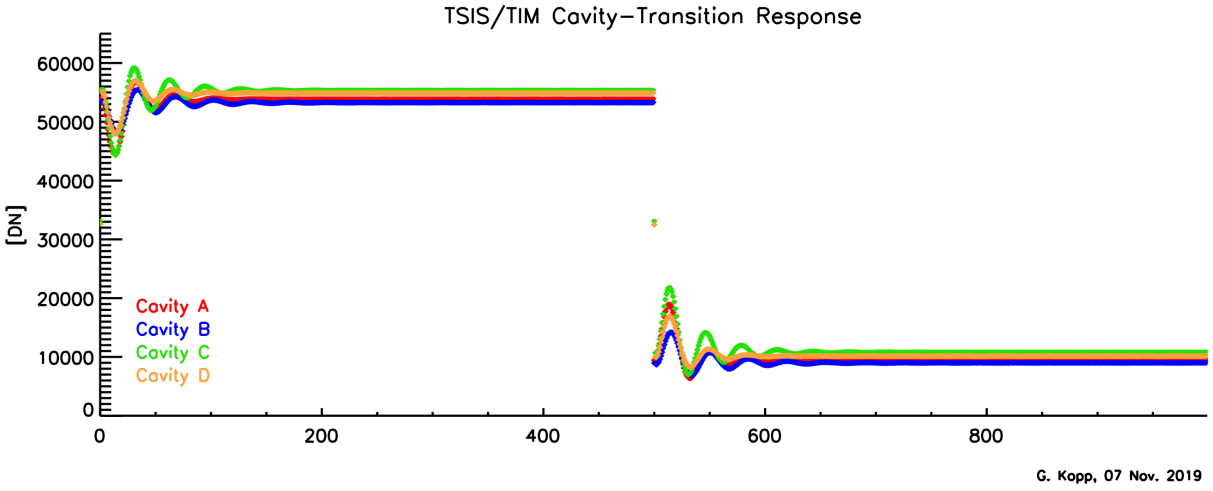

Figure 2: Observed transients differ for each TSIS-1/TIM cavity, indicating different thermal responses (and associated equivalence values) in each. These variations lead to the observed differences between the TSI values computed for each cavity in early-mission data versions, which assumed the same equivalence value for all channels.

4 Measurement Equation(s) and Definitions of Terms

Two measurement approaches are described here. The PSD method has been used for the SORCE, TCTE, and TSIS-1 TIMs and has several benefits, especially for the former two instruments. This method was initially described in the SORCE ATBD [8]. A DCS method similar to those used in ground-based laboratory measurements has also been

applied now to the TSIS-1/TIM to help resolve cavity-to-cavity differences. The PSD and DCS methods are described in §4.1 and §4.2, respectively.

4.1 PHASE SENSITIVE DETECTION (PSD)

The active TIM ESR's bistable shutter is cycled 50% open and 50% closed with a 100-second period (0.01 Hz) to acquire observations. Only the variations in electrical replacement heater power that are in-phase with this shutter fundamental are analyzed. This phase-sensitive detection method suppresses the instrument's susceptibility to noise, the radiative thermal background, and out-of-phase but synchronous time-varying fluctuations in temperatures, enabling this ambient-temperature radiometer to achieve high accuracy and low noise.

The PSD-based TIM measurement equation is unchanged from that in the original TSIS-1 ATBD. The measurement equation follows from the signal flow diagram shown in Figure 3. The equation is reproduced in Eqn. 1 with respective terms described below. For a full description and background, see [1].

The PSD-based TIM measurement equation is

Eqn. 1 $$E_{meas} = \frac{V^2}{64000 \cdot R_{eff}} \cdot \frac{1}{A_p} \cdot \frac{1}{\alpha} \cdot Re\left\langle \frac{1}{\psi} \cdot \left[-DN_{meas} \left(1 + \frac{1}{G}\right) + DN_{FF} \cdot \frac{1}{G} \right] \cdot \frac{Z_H}{Z_R} \right\rangle$$

where

- E_{meas} is the measured irradiance
- V is the applied voltage
- R_{eff} is the cavity-heater resistance
- A_p is the aperture area (including diffraction-loss, temperature, and pressure corrections)
- α is the cavity absorptivity
- Ψ is the shutter waveform
- DN is the data number value for the measurement (*meas*) or for the applied feedforward (*FF*), and is applied as a value digitized over 64000 steps (hence that value in the denominator in Eqn. 1)
- G is the servo-system gain
- Z_H/Z_R is the non-equivalence of heater to radiative power absorbed

The last four items in this list are represented as complex phasors. While these are functions of frequency, the only relevant frequency needed here is that of the shutter fundamental.

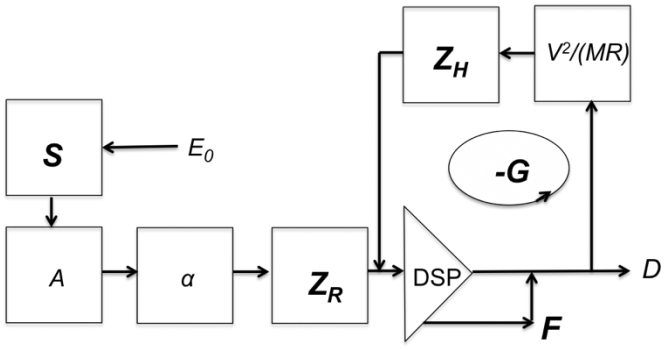

Figure 3: Signal flow diagram for the TIM instrument. Variables in boxes are out/in ratios at some frequency. The servo loop gain is **–G**. The digital signal processor (DSP) adds a known feedforward signal **F**. The ratio of thermal impedances Z_H/Z_R is the equivalence ratio. **Bold** symbols represent complex phasors. (Reproduced from Kopp and Lawrence 2005 [3].)

The value given by the instrument-intrinsic measurement in Eqn. 1 is corrected for thermal background measurements (E_{dark}) acquired by viewing dark space, on-orbit degradation in sensitivity, and external factors by the equation

Eqn. 2
$$E_{Sun} = \frac{1}{f_{AU} f_{Doppler} f_{point} f_{degrade}} \cdot [E_{meas} - E_{dark}]$$

where

- f_{AU} is the correction for spacecraft distance to the Sun
- $f_{Doppler}$ is the correction for spacecraft line-of-sight velocity relative to the Sun
- f_{point} is the sensitivity of the instrument to incidence angle
- $f_{degrade}$ accounts for changes in instrument response with time through the mission

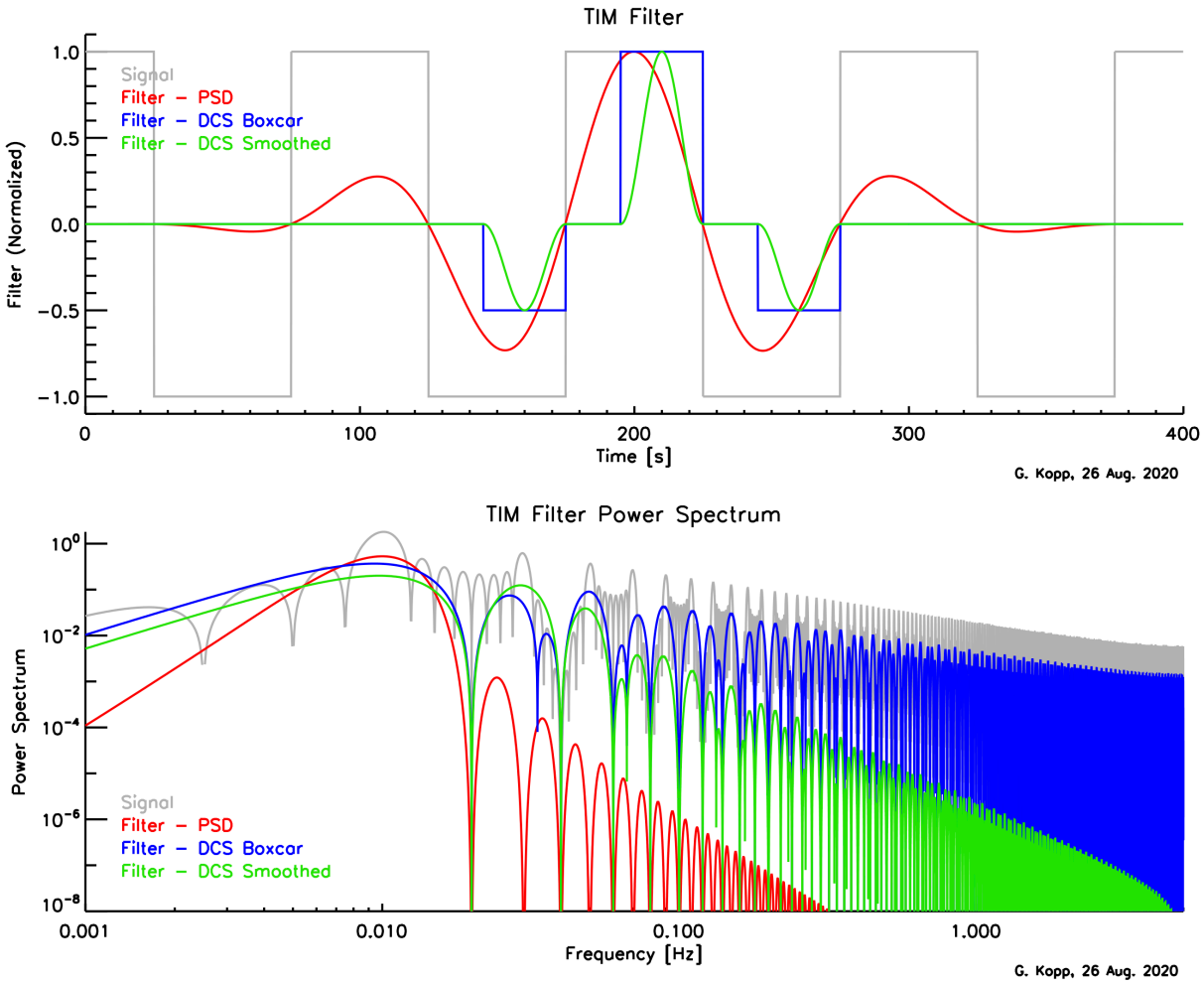

Figure 4: TIM filters for PSD (red) and Hanning-smoothed DCS (green) are shown with the shutter signal (grey) and a 30-second boxcar weighting (blue) used in the DCS (top plot). Normalized power spectra of the same filters (bottom plot) show the high-frequency suppression, which is particularly strong for the PSD filter.

The TIM data-processing systems for the SORCE, TCTE, and TSIS-1 have used a measurement kernel consisting of a 100-second boxcar average applied four times and weighted by 0.01-Hz sinusoidal components, as shown in the red curve in the top plot of Figure 4 and described in [3] and [8]. With the finite duration of this kernel, the PSD analysis

actually includes a range of frequencies rather than just those at 0.01 Hz, as shown in red in the bottom plot of Figure 4 via the power spectrum of this PSD filter.

The disadvantage of the PSD analysis is that all data throughout each shutter cycle are used, including the transients near shutter transitions. Corrections affecting those transients, such as servo-system gain (~2100 ppm), non-equivalence (~1200 ppm), and shutter waveforms (~50 ppm), must therefore be very accurately known, as described in §3.3. Uncertainties in these values can cause decreased accuracy in order to achieve lower noise via the PSD method.

The TIM instrument, particularly its thermal-stability and servo-control systems, have been designed to reduce noise at the shutter fundamental of 0.01 Hz. An instrument-noise power spectrum using one extended day of flight data is shown in Figure 5. This noise power spectrum reaches a broad minimum near 0.004 Hz. The 0.01-Hz shutter fundamental was chosen to be near – but at a slightly higher frequency than – this minimum. This maintains now noise while enabling faster instrument cadences. Note that the data-processing filters (shown in Figure 4) all reach a maximum sensitivity at this chosen shutter frequency. The effects of increases in noise power on either side of this fundamental can be reduced via selecting filters that sharply increase their suppression of these out-of-band frequencies. The PSD filter (shown in red in the bottom plot of Figure 4) has the best such suppression for both higher and lower frequencies.

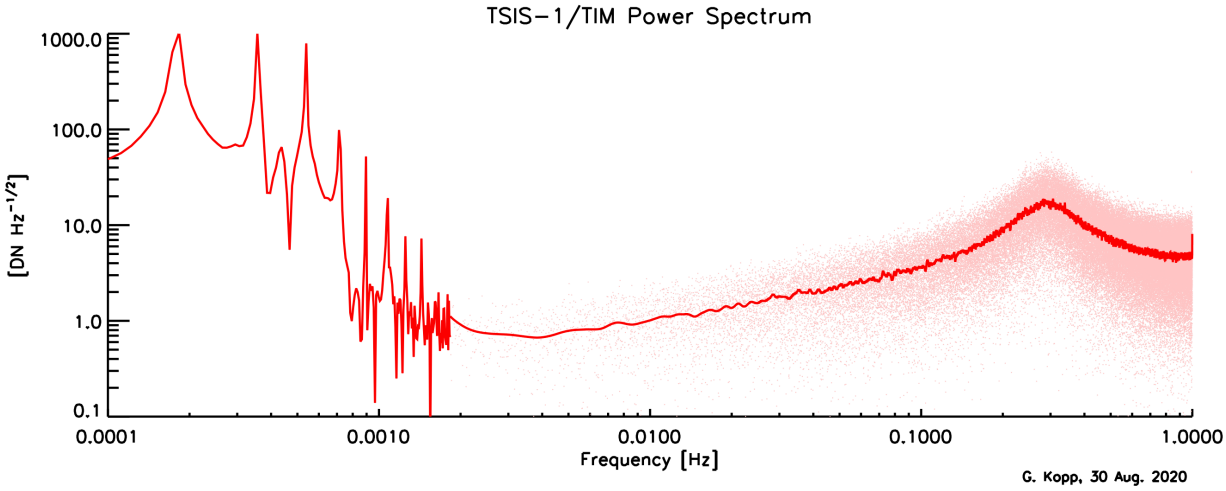

Figure 5: The TSIS-1/TIM noise power spectrum is near a minimum at the 0.01-Hz shutter fundamental, helping the instrument achieve extremely low measurement noise. Data in the plot are smoothed above 0.0018 Hz for clarity. Noise power increases at lower frequencies are mainly due to thermal variations. The peak at 0.175 mHz is due to orbit-period variations.

4.2 DC Subtraction (DCS)

The DCS technique provides much better cavity-to-cavity agreement than the PSD for the TSIS-1/TIM because it excludes the shutter-transition transients, which are due to large (but improperly known in V.1 and V.2 data releases) non-equivalence ratios. There are no changes to the TIM operations whether PSD or DCS is used, so instrument telemetry captured can be reprocessed using either PSD or DCS. V.3 data use a hybrid combination of both algorithms.

The DCS measurement equation is given by

Eqn. 3
$$E_{meas} = \frac{V^2}{64000 \cdot R_{eff}} \cdot \frac{1}{A_p} \cdot \frac{1}{\alpha} \cdot (-DN_{meas})$$

where DN_{meas} is now an average over some defined subset of the instrument data (as detailed below in this section and with the general solution given by Eqn. 5). Note that, compared to the PSD measurement equation given by Eqn. 1, this equation utilizes only scalars. The same additional corrections given by Eqn. 2 are still applied.

The advantages of the DCS approach vs. PSD include

1. Can improve absolute accuracy by reducing reliance on the knowledge of the AC equivalence ratio
2. Simplifies the measurement equation by eliminating the time-dependent phasors

while the disadvantages are

1. Higher noise at almost all frequencies
2. Susceptibility to potential out-of-phase thermal effects

If all calibration terms are correctly implemented, the TSI values from the PSD and DCS algorithms should agree. That they do not in V.1 and V.2 TSIS-1/TIM data indicated a problem traceable to an incorrectly-known AC equivalence ratio.

4.2.1 DCS Boxcar-Type Filter

In the DCS approach, once a stable DC level is reached after a shutter transition, the subsequent data for that shutter state are averaged. The difference between the averaged shutter-open and -closed levels determines the radiant-power signal level. By not using the transient-response data immediately following a shutter transition, the DCS analysis is very insensitive to uncertainties in the gain, shutter waveform, and equivalence ratio, all of which affect this transient.

The simplest example of a DCS filter would be a boxcar average over equal portions near the end of the half-cycles of one shutter-open and one shutter-closed state, subtracting the closed-state average from that of the open state. This is the approach used by all TSI instruments prior to the TIM, including the ACRIM and VIRGO instruments. A slightly more sophisticated and symmetrical filter would equally balance a center shutter-state by the alternate state on both sides. An example of this three-half-cycle boxcar-type filter is shown in the blue curve in the top plot in Figure 4. This boxcar-type filter can be generalized to any number of half-cycles (which need not even be an integer number) and any fraction of the half-cycle.

Note that the DCS boxcar-type filter shown in Figure 4 gives the worst out-of-band suppression of noise of any of the plotted filters.

4.2.2 DCS Filter with Smoothing Function

The DCS boxcar-type filters suffer from significant contributions from high-frequency noise, as shown by the blue curve in the power spectrum of the three-half-cycle boxcar-type filter in the bottom plot in Figure 4. A smoothing of the edges on the boxcar-type filters reduces this noise, which helps suppress the increasing instrument noise at frequencies higher than the shutter fundamental (see Figure 5). A Hanning function such as given by Eqn. 4 is one possible means of such smoothing. Other such smoothing functions include Hamming, Blackman, etc. Although the differences between these are small, they and other smoothing methods could be considered for future DCS-based data-analysis filters.

The Hanning smoothing used here is given by

Eqn. 4
$$w_i = \frac{1}{2}\left(1 - \cos\left(\frac{2\pi i}{N-1}\right)\right)$$

where

- N is the total number of DNs used per half-cycle after excluding the points near the shutter transition
- i is the index of the used DN points in a half-cycle

The improvement this Hanning-smoothed DCS filter provides compared to the three-half-cycle boxcar-type filter is illustrated by the green curve in the bottom plot of Figure 4. However, it is also important to note the further noise-reduction improvements provided by the PSD method (shown in red).

4.2.3 DCS Filter – General Case

For a DCS approach with an arbitrary (but integer) number of equally-weighted half-cycles, an incoming time series, DN_{hi}, is processed to provide the real output series DN_{meas} via the weighted average

Eqn. 5
$$DN_{meas} = \left(\sum_{h=0}^{H-1} \sum_{i=0}^{N-1} \frac{DN_{hi} \cdot w_i \begin{cases} -1, s_h = 1 \\ 1, s_h = 0 \end{cases}}{\begin{cases} \lceil H/2 \rceil, s_h = s_0 \\ \lfloor H/2 \rfloor, s_h \neq s_0 \end{cases}} \right) \Big/ \sum_{i=0}^{N-1} w_i$$

where

- H is the number of half-cycles used (nominally 3 for the TSIS-1 DCS approach)
- s_h is the shutter state for half-cycle h (1=open, 0=closed)

Variable parameters in the DCS approach for the most general case include

1. The number H of half-cycles sampled
2. The stabilization (or "delay") time needed after each shutter transition
3. The smoothing function w applied

4.2.4 Determining DCS Stabilization Times

The needed stabilization time (i.e. the number of data points ignored after each shutter transition) can be determined by analyzing irradiance data using increasing stabilization times. Once stabilization times are long enough to mask the effects of transients, resulting computed values should be consistent with those from subsequent increases in stabilization times (until noise from having too few data points at the longer stabilization times dominates). The results of this analysis are shown in Figure 6 using a three-half-cycle Hanning-smoothed DCS analysis.

A stabilization time of 0 utilizes the entire shutter cycle, so can include systematic erroneous effects due to the shutter transition. A stabilization time approaching the full length of the shutter half-cycle may allow for the best servo-system stability to be achieved but leaves fewer data points to average, so is more susceptible to random noise, as indicated by increasing standard deviations (shown by the pink shaded region and the red curve in Figure 6). A minimum is reached at intermediate times. At stabilization times of 10 % of the half-cycle, the value measured is within 10 ppm of the intermediate stabilization-time values. By ~40 % (20 seconds), the transient has essentially no effect and random-noise-limited end effects are insignificant. Intermediate delay times from ~20 % to ~60 % of the half-cycle show the most stability, having < 3 ppm variability.

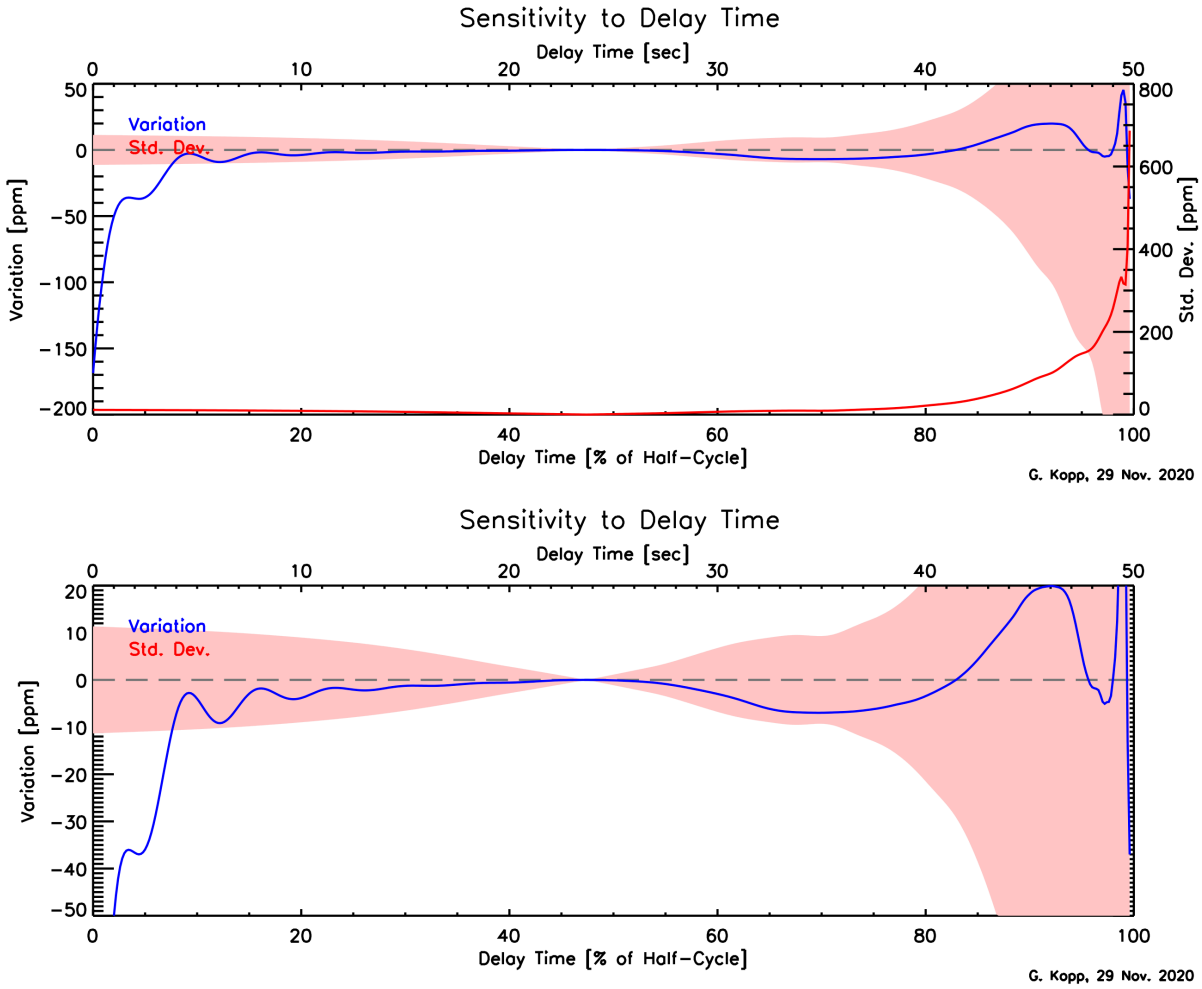

Figure 6: By repeating data analysis using a three-half-cycle Hanning filter with different stabilization times, a range of useable delay times can be determined. This range includes times after which transients have damped out but before random-noise effects become important. The blue and red curves (and the pink shaded regions) respectively show the variation in the irradiance means and the standard deviations from several shutter cycles during one orbit compared to a baseline 23.7-second delay time. (A baseline is needed to discern these small variations in standard deviations over that of the large intrinsic solar variability.) The bottom plot shows the plot on an expanded scale.

4.2.5 Current TSIS-1/TIM Implementation of DCS Filter

As currently implemented for the TSIS-1/TIM, the instrument's DCS algorithm replaces the PSD kernel with a weighted average of three shutter half-cycles with the first and third being negatively weighted relative to the intermediary and a Hanning function applied, as shown by the green curve in the top plot of Figure 4. In this implementation, a 20-s delay after the shutter transition at the beginning of each 50-s half-cycle is excluded (see §4.2.4).

4.2.6 Further Parameter Considerations for DCS Filters

Eliminating the hard edges of the filters significantly reduces the high-frequency response of the filter, and thus reduces the noise relative to a boxcar-type filter. Noise can be further reduced by extending the number of cycles for the filter, similar to the PSD filter. A four-cycle (more accurately, seven half-cycles in this case) filter with a total

duration of 350 seconds is shown in Figures 7 and 8. The benefits of these smoothing and lengthening approaches on noise are quantified in §4.3.

Noise reductions via lengthened filters must be weighed against the resulting losses of useable data from solar-observing periods, as the lengthened filters require longer periods of uninterrupted observations. These can be particularly restrictive in operating environments with limited observing, such as on the ISS or during TIM field-of-view map characterizations from low-Earth-orbiting spacecraft, which have limited-duration sunlit orbit portions.

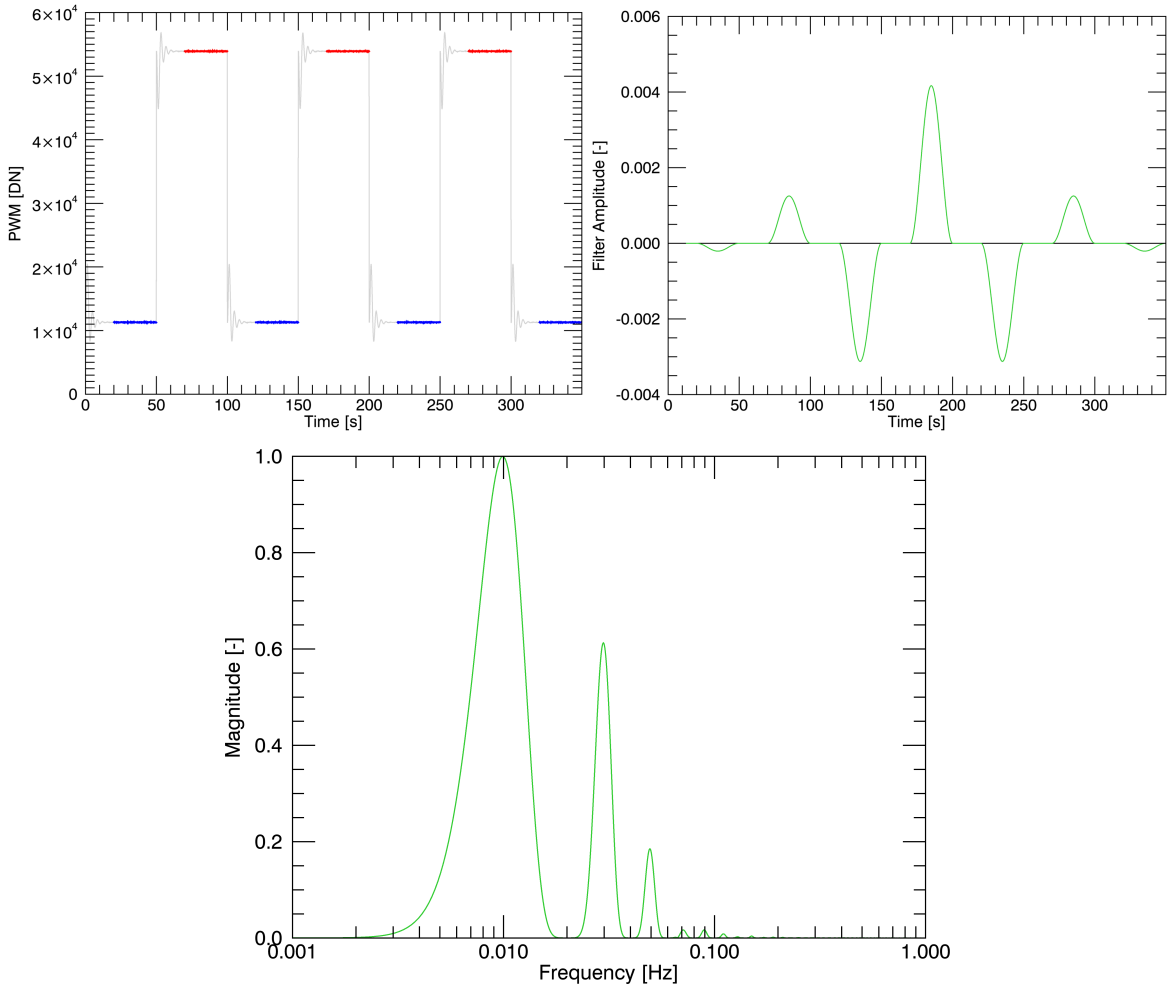

Figure 7: A seven-half-cycle symmetric Hanning-smoothed DCS filter is a better match to the PSD kernel in that it also uses four shutter cycles, as shown in the top plot in Figure 4. We show it here as a potential filter for future DCS implementations. The top left plot shows the data sampled. The top right plot shows the filter weighting with time and the bottom plot shows the filter's power spectrum. Even this four-cycle filter has greater high-frequency noise susceptibility than that of the PSD kernel (see bottom plot in Figure 4).

4.3 Noise Comparisons

Any filter used for the TIM should have much lower noise than the intrinsic short-term solar-caused variations of the TSI, which is > 20 ppm over the sunlit portion of an orbit (see [6]). To characterize the noise of various filters, several different types, shown in Figure 8, were applied to on-orbit data taken with the TSIS-1/TIM primary cavity (A) while the shutter was closed. (These are the same data from which the power spectrum in Figure 5 was computed.) The modulated input power is zero, so the standard deviation of the measured signal gives the intrinsic instrument noise.

The results are shown in Table 1 and plotted in Figure 9. The three-half-cycle DCS boxcar-type filter has nearly three times greater noise than the PSD filter, while a seven-half-cycle Hanning filter gives a little less than twice the noise of the PSD filter. A three-half-cycle Hanning filter gives just over twice the noise of the PSD filter while providing advantages in length of data required per result. All filters thus meet the TIM noise requirements.

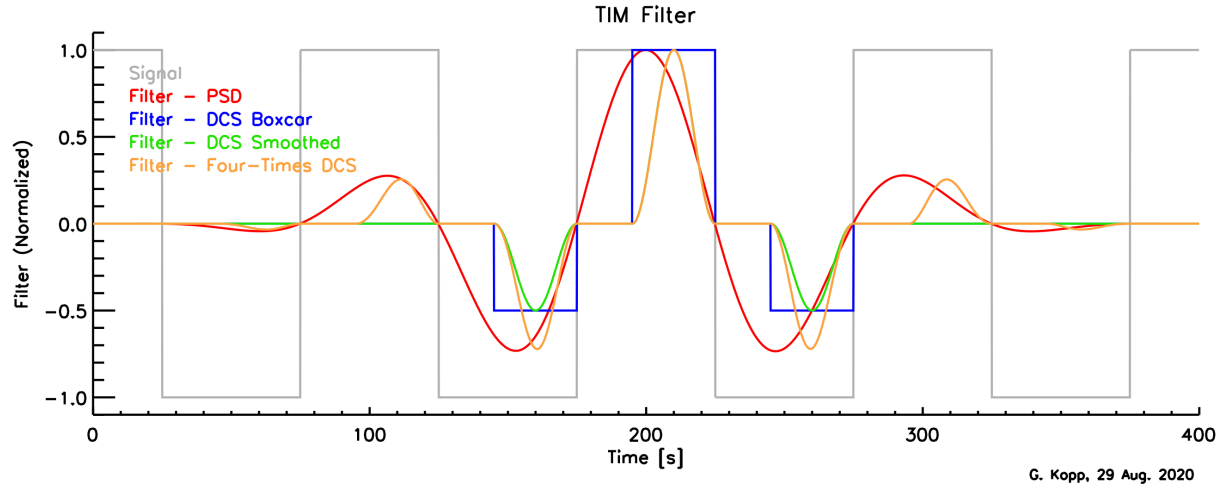

Figure 8: Instrument noise was compared using four different filters: the standard PSD filter (red), a three-half-cycle DCS boxcar filter (blue), a Hanning-smoothed three-half-cycle DCS filter (green), and a four-cycle (seven-half-cycle) Hanning-smoothed filter (orange).

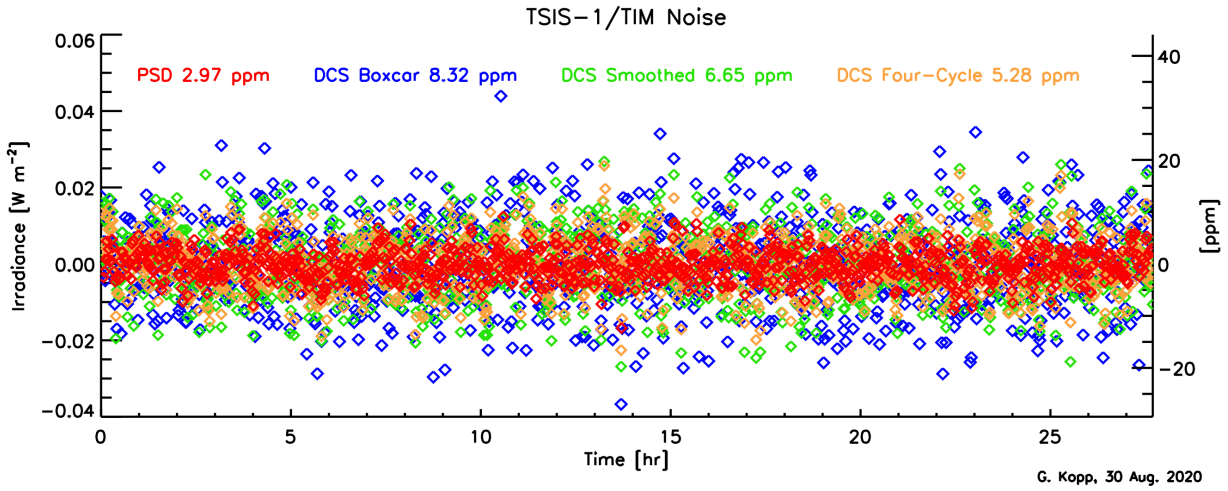

Figure 9: Computed instrument noise for the filters shown in Figure 8. Results are tabulated in Table 1.

Table 1: Measurement Noise for Different Filters

Filter	Length [cycles]	Length [s]	Noise [ppm]
DCS Boxcar	3 half-cycles	150	8.32
DCS - Smoothed	3 half-cycles	150	6.65
DCS - Smoothed	4 cycles	350	5.28
PSD	4 cycles	400	2.97

5 TSIS-1/TIM Science Data

5.1 Science Data System

The TIM science data system (SDS) has been updated to support the two different processing algorithms without introducing unnecessary duplication in the software. The core software is largely the same as what was previously used with the SORCE [8], TCTE, and TSIS-1 TIMs. Figure 10 outlines the core processing steps and how data flow between them. Note that most steps are common to both algorithms. Steps identified as having two algorithm-specific implementations were abstracted to a standard interface in order to allow for the DCS implementations. Steps with only a PSD identifier are not required when processing with the DCS method, simplifying the science algorithm and improving processing performance.

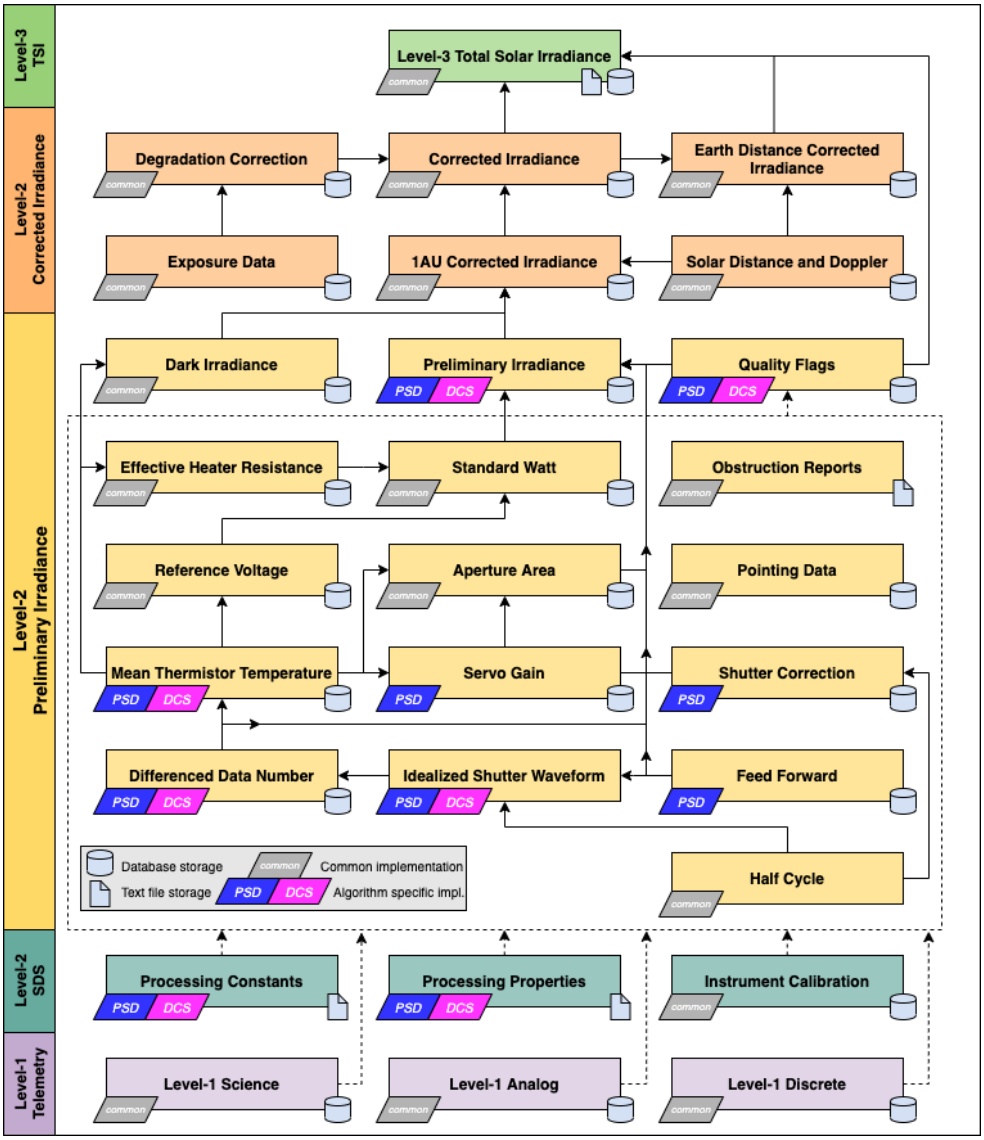

Figure 10: TSIS-1/TIM data-flow diagram for the PSD and DCS methods. The differences between processing algorithms are identified by the PSD and DCS labels. The data flow for the Level-1 telemetry, Level-2 SDS, and quality flags is not shown.

The static inputs to the SDS are the processing constants, processing properties, and instrument calibration parameters. Processing constants are defined at compile time for a data release and include processing strategy (i.e. PSD or DCS), half-cycle duration, and half-cycle count. Processing properties are defined in a text file that is loaded at processing runtime and includes mission name, a set of calibration versions, the data-release version, and database connection parameters. Instrument calibration data are stored in a mission-specific database that is accessed by all data releases. Each calibration dataset can contain multiple versions in order to support in-flight calibration updates. The calibrations are not specific to a processing algorithm, although an algorithm might not use every type of calibration (e.g. DCS does not use the equivalence-ratio calibration).

5.2 TSIS-1/TIM V.3 DATA

V.3 is the third public release of TSIS-1/TIM data and the first to use a hybrid-PSD analysis approach, with the DCS providing non-equivalence calibration values that improve the absolute accuracy and cavity-to-cavity agreement while the PSD approach maintains lower noise and heritage with prior data versions and TIM instruments. These data meet all mission threshold requirements. The calibration updates in this release have improved the stated uncertainties from those in prior versions particularly in regard to the absolute-value uncertainties. These were greater in V.1 and V.2 largely due to the intra-instrument cavity-to-cavity differences caused by using the Glory non-equivalence value for all cavities in those earlier data versions. The uncertainty due to these cavity-to-cavity differences is 66 ppm as of the initial production of V.3 (in April 2020).

The V.2 Level-2 data from the mission for the PSD method prior to applying new corrections for non-equivalence is plotted in Figure 11. The relative cavity differences are

```
Intercomparison Differences:        A-B       A-C       B-D       A-D
                             -0.563846  0.759224  0.406827 -0.156397 W m^-2
                               -414.29    557.84    298.92   -114.91 ppm
Unweighted Mean of Offsets from Primary Cavity: -0.009590 W m^-2     -7.05 ppm
Unweighted Standard Deviation of Offsets:        0.553363 W m^-2    406.59 ppm
(updated 9 Apr. 2020)
```

The unweighted standard deviation of the cavity offsets is the largest contributor to the stated uncertainties for V.2. Applying the DCS method with a three-half-cycle Hanning filter gives the improved cavity-to-cavity differences shown in Figure 12. These DCS-based cavity differences are

```
Inter-Comparison Differences:       A-B       A-C       B-D       A-D
                             -0.110658 -0.069491  0.205982  0.095280 W m^-2
                                -81.31    -51.06    151.35     70.01 ppm
Unweighted Mean of Offsets from Primary Cavity:  0.021206 W m^-2     15.58 ppm
Unweighted Standard Deviation of Offsets:        0.090115 W m^-2     66.21 ppm
(updated 9 Apr. 2020)
```

V.3 uses the DCS method to derive the non-equivalence value of each cavity needed to make the PSD- and DCS-computed values (as shown in Figures 11 and 12, respectively) agree. The non-equivalences thus derived are

```
Cavity A: (1.0010680d, 0.01394351d)
Cavity B: (1.0007340d, 0.01393886d)
Cavity C: (1.0016762d, 0.01395198d)
Cavity D: (1.0008783d, 0.01394087d)
```

These are then implemented in the PSD-based measurement equation, maintaining the low-noise advantages and the heritage of that approach while benefitting from the accuracy of the DCS approach via the on-orbit-derived non-equivalence values above. The full-mission Level-3 TSI results using this hybrid-PSD approach are shown in Figure 13.

The PID coefficients for the instrument's closed-loop heater-control servo system regulating the cavities were adjusted on 9 April 2018, reducing noise in subsequent measurements. Note in Figure 12 that the DCS method is much more susceptible to this earlier-mission noise than the PSD method, which provides increased motivation for the hybrid-PSD approach of V.3.

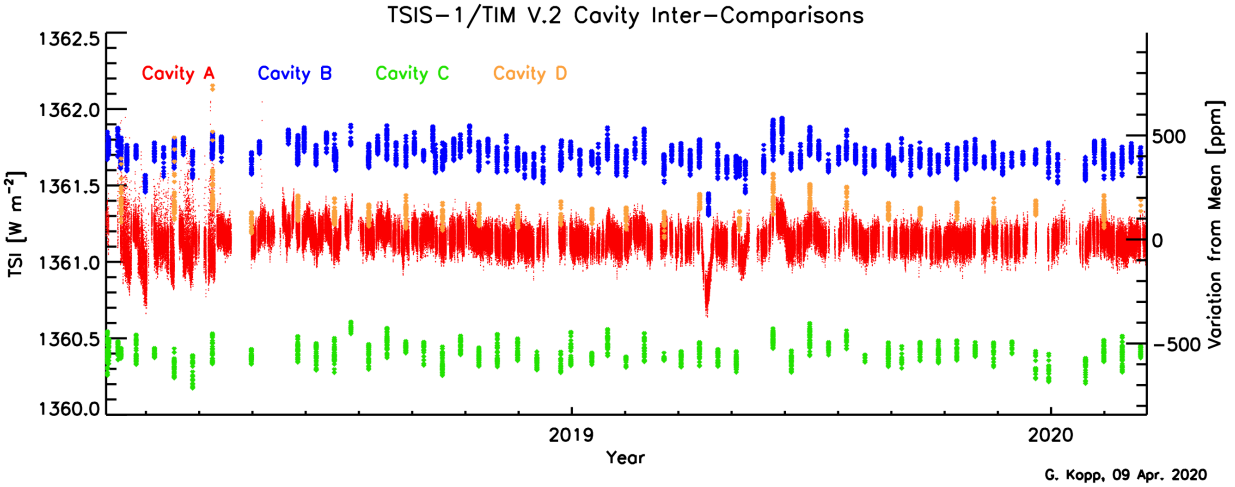

Figure 11: V.2 Level-2 corrected irradiance analysis results are shown for the PSD approach. The 50-second cadence samples for the primary cavity (shown in red) are used to produce the Level-3 daily and 6-hourly TSIS-1/TIM TSI values given in publicly-released data. These data, as with V.1, utilize the Glory/TIM non-equivalence values, which cause the large inter-cavity differences. Those differences are given in the text above.

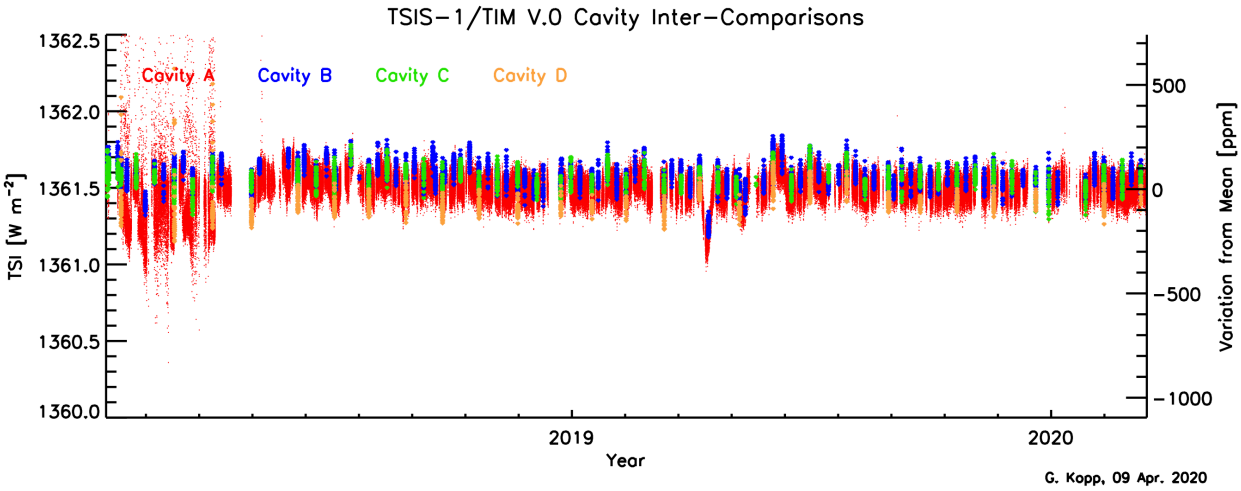

Figure 12: Using the DCS method with a three-half-cycle Hanning filter gives the improved inter-cavity agreement shown here but comes at the expense of higher noise. Cavity differences for these data are given in the text above.

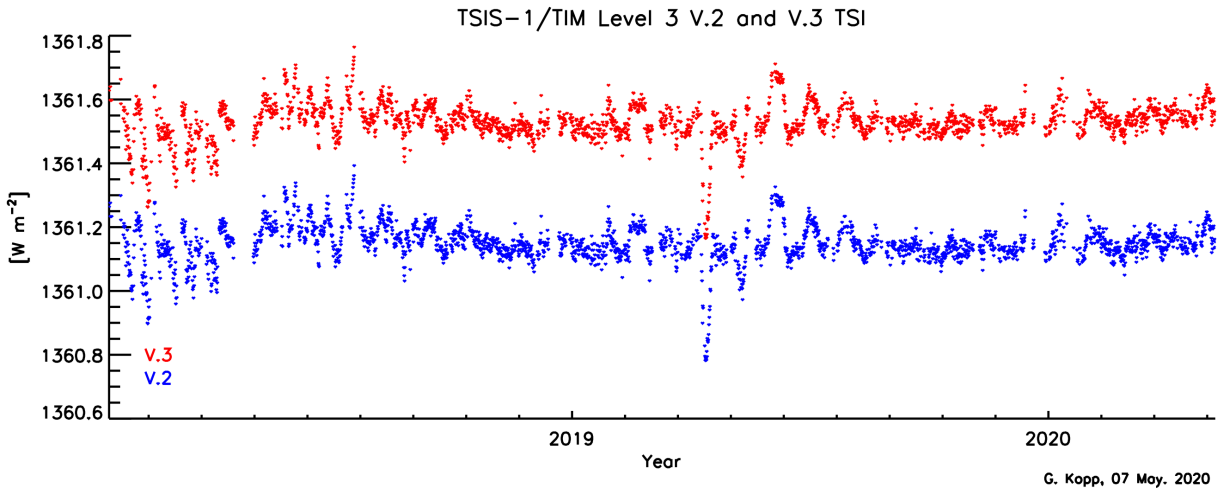

Figure 13: The Level-3 V.3 data are more accurate than – and still within the stated uncertainties of – those of the prior data version. Most data gaps are due to ISS activities that limit TSI observations.

5.3 UNCERTAINTY ESTIMATES

In listing uncertainties, this ATBD consistently quotes "relative standard uncertainty" in units of ppm, or 10^{-6}. "Relative" refers to a fractional uncertainty, "standard" indicates a 1-σ standard deviation, and "uncertainty" means a lack of knowledge of the indicated parameter. Since the individual uncertainty contributors are considered to be independent, the instrument's net uncertainty is given by the root sum square (RSS) of all the contributing uncertainties.

The uncertainty budget for the TSIS-1/TIM is provided in Table 2. Type A and B uncertainties are distinguished as possible. This budget is focused on the PSD method, but largely encompasses the parameters in the DCS method as well. The parameters "Shutter Waveform," "Non-Equivalence," and "Servo Gain" are specific to the PSD analysis method; although the DCS method will still have a DC non-equivalence parameter. "Measurement Repeatability (Noise)" would be higher in the DCS, but not substantially (see §4.3).

While the DCS method has lower uncertainties for absolute accuracy, much of that can be transferred to the PSD analysis via the non-equivalence values, as done for V.3. This hybrid-PSD method, albeit still having slightly higher uncertainties due to the additional parameters included in its measurement equation (and in Table 2), offers improved noise. Since that noise is relevant on short-term timescales, which are useful for solar studies involving oscillations and convection, flares, and planetary transits, none of which are concerned with absolute accuracy, the hybrid-PSD method used in V.3 is the currently-preferred analysis method for its noise characteristics, DCS-based accuracy, and heritage. The PSD method, however, is more sensitive to pointing variations. These are being characterized using field-of-view maps throughout the mission but require multiple maps to build up pointing sensitivities. Placeholder uncertainties are included currently in Table 2 for this parameter and for sampling, both of which will be refined throughout the TSIS-1 mission as more data are acquired.

The instrument's uncertainty increases monotonically with time after the initial measurements, as on-orbit degradation, component aging, and uncharacterizable space-environment effects can decrease the certainty of the ground-based calibrations with time. Examples include drifts in the instrument's two voltage or four heater-resistance references, cavity degradation with exposure to unfiltered UV and X-rays from the Sun, radiation damage from high-energy electrons and protons, contamination due to spacecraft or instrument materials, and changing emissivities of instrument surfaces. A jump in mid-2019 corresponds with inconsistencies in cavity inter-comparisons. For V.3 data,

stability estimates of < 16 ppm yr^{-1} (see footnote[1]) are summed in quadrature with the initial absolute-accuracy uncertainty to indicate the time-dependent uncertainty in the TIM's measurements.

Table 2: TIM Uncertainty Budget

Correction Parameter	Value [ppm]	Type A	Type B	Channel A	Channel B	Channel C	Channel D
Distance to Sun, Earth & S/C	*33,537*	*0.1*		*0.1*	*0.1*	*0.1*	*0.1*
Doppler Velocity	*57*	*0.7*		*0.7*	*0.7*	*0.7*	*0.7*
Shutter Waveform	50	0.5		*0.5*	*0.5*	*0.5*	*0.5*
Aperture	*1,000,000*		23	*23*	23	22	23
Diffraction	*452*		*14*	*14*	*14*	*14*	*14*
Scatter	*9*		1	*1*	1	1	9
Cone Reflectance	*186*		*40*	*40*	*55*	*84*	*41*
Non-Equivalence, ZH/ZR - 1	*1,165*		*58*	*58*	*42*	*89*	*49*
Servo Gain	*2,134*	*0.9*		*0.9*	*0.7*	*0.7*	*0.9*
Standard Volt + DAC	1,000,000		11	*11*	*11*	*11*	*11*
Pulse Width Linearity	800		7	*7*	*7*	*7*	*7*
Standard Ohm + Leads	1,000,000		32	*32*	*32*	*32*	*32*
Dark Signal	1,775		9	*9*	*9*	*9*	*9*
Pointing			*40*	*40*	*40*	*40*	*40*
Measurement Repeatability (Noise)		4		*4*	*4*	*4*	*4*
Uncertainty due to Sampling		*30*		*30*	*30*	*30*	*30*
Inter-Cavity Agreement	66			*59*	*59*	*59*	*59*
Total RSS		***30***	***93***	***114***	***113***	***151***	***110***
orange values are current estimates							

The individual and net effects of these uncertainty contributions are plotted in Figures 14 and 15 and reported in the released Level-3 data products. The initial absolute-value uncertainty shown is currently ~10 % more conservative than those results in Table 2.

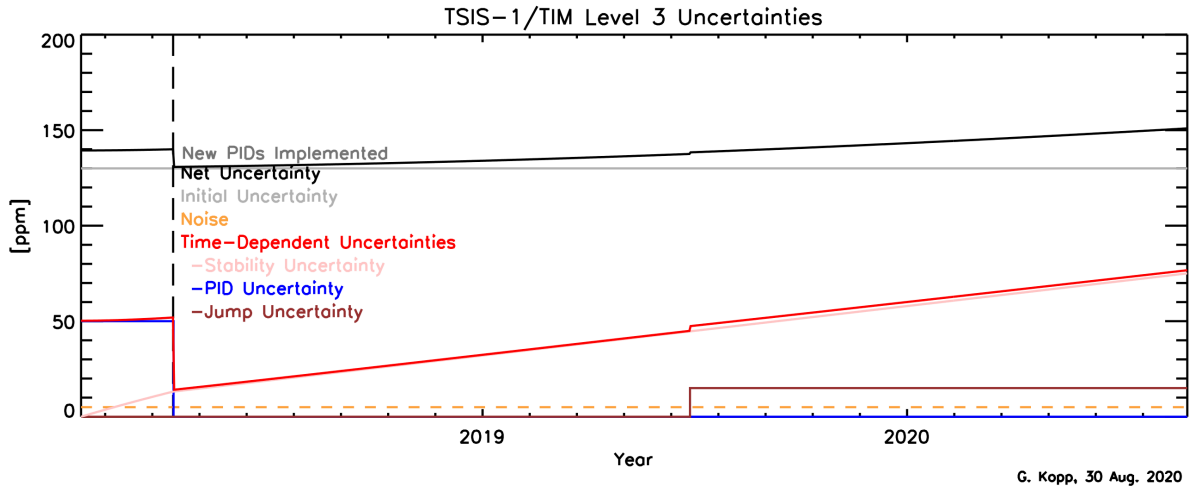

Figure 14: The net TSIS-1/TIM estimated uncertainties for V.3 data are well below the threshold requirements for accuracy.

[1] This may be an overestimate of the uncertainty growth with time, as suggested by a 1/*f* dependence described by [2].

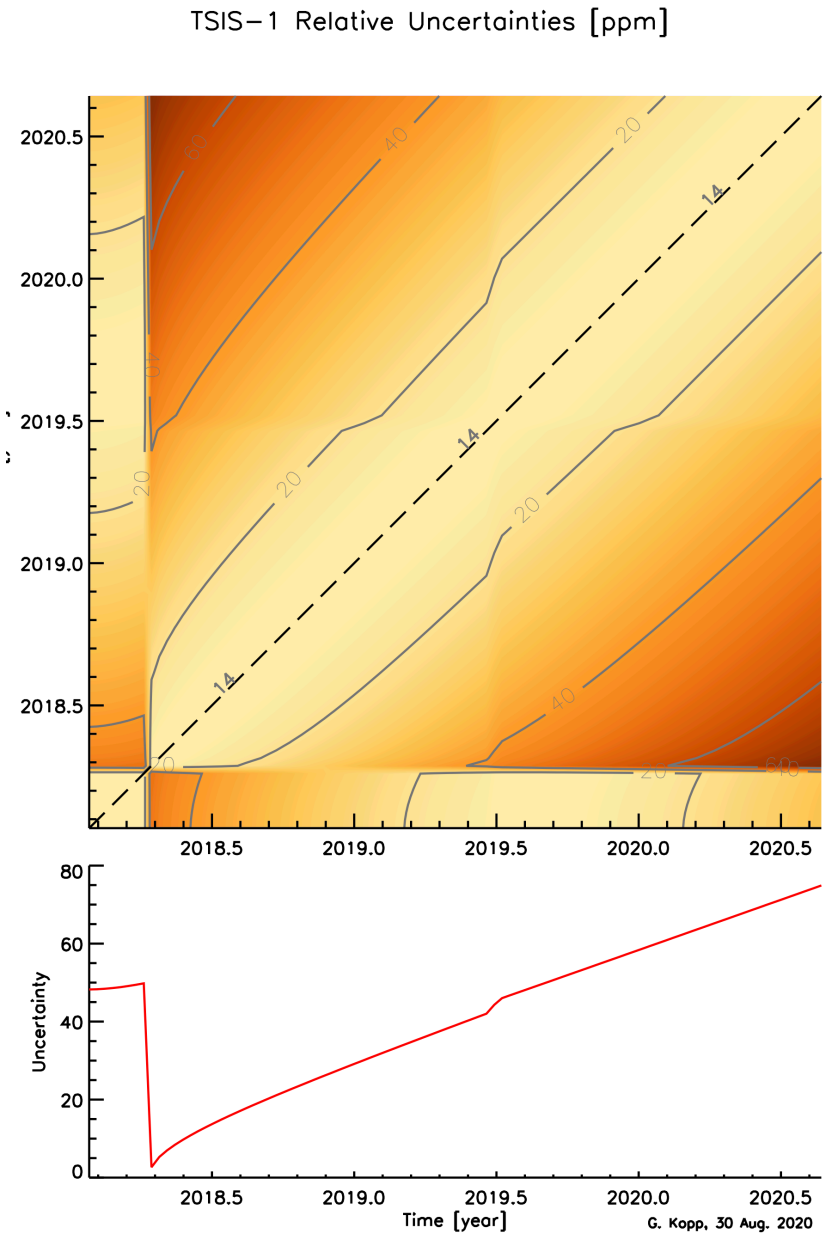

Figure 15: Uncertainties are better represented in two dimensions in order to more easily visualize the relative differences between any two times. This plot shows the total time-dependent uncertainties from Figure 14 to indicate temporal regions in which relative TSI changes have low uncertainties. This is useful for solar-variability comparisons between two times using this one TIM data set.

6 Validation

6.1 Validation Philosophy

The TIM is a primary radiometer. It is not cross-calibrated from any other TSI instrument on-orbit. To maintain independence between all TSI instruments, the TSIS-1/TIM data products do not rely on any other instrument measurements. The findings and corrections presented in this ATBD were acquired purely via intra-instrument cavity comparisons.

This has not been the case with some other TSI instruments. Such cross-calibrations, however, can cause measurement consistency between separate instruments, which can erroneously be considered as validations of each. This has particularly been an issue with the SoHO/VIRGO, which formerly relied on other on-orbit instruments to determine intra-VIRGO allocations of degradation corrections.

The SORCE, TCTE, and TSIS-1 TIM data maintain complete independence from each other and from all other instruments.

6.2 COMPARISONS WITH OTHER TIM INSTRUMENTS

The TSIS-1/TIM overlapped temporally (and temporarily) with the predecessor TIMs on the SORCE and TCTE, as shown in Figure 16. The short-term variations in this plot are due to actual solar-irradiance variations, and, as should be expected, are therefore common-mode between the three instruments despite their different spacecraft platforms and slightly different observing times. The scale differences between the three are small, as indicated in ppm on the right-hand vertical axis, and the three agree within their stated uncertainties. Achieving this level of agreement is a necessary but not sufficient condition of the three independently-calibrated instruments' stated uncertainties being realistic and of these values reflecting the actual TSI level at these times.

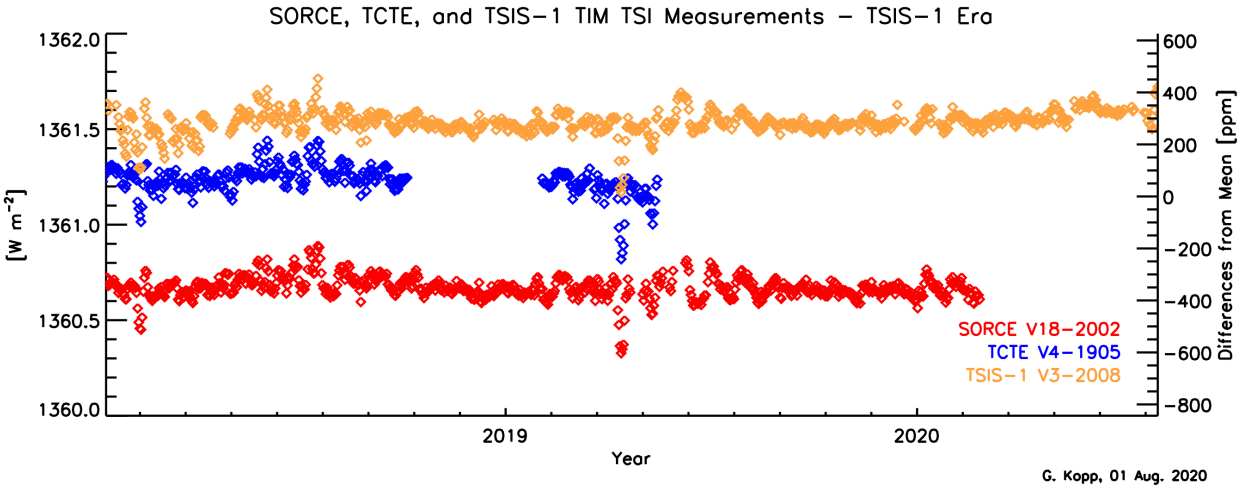

Figure 16: The SORCE, TCTE, and TSIS-1 TIMs overlapped near the beginning of the TSIS-1 mission. Shown here are the overlapping values during the TSIS-1 era. Each instrument shows similar short-term changes, which are due to variations in solar activity and hence are common mode. On an absolute scale, the three instruments agree within their stated uncertainties. These Level-3 data from the three TIMs are not adjusted in any way to each other. (Data and plot are updated regularly at [7].)

7 References

1. Coddington, O., TSIS-1 Algorithm Theoretical Basis Document, https://disc.gsfc.nasa.gov/datasets?keywords=TSIS&page=1, 2017
2. T. Dudok de Wit, G. Kopp, C. Fröhlich, and M. Schöll, "Methodology to create a new Total Solar Irradiance record: Making a composite out of multiple data records," *Geophysical Research Letters*, 2017, doi:10.1002/2016GL071866
3. Kopp, G. and Lawrence, G., "The Total Irradiance Monitor (TIM): Instrument Design," *Solar Physics*, 230, 1, Aug. 2005, pp. 91-109, doi:10.1007/s11207-005-7446-4
4. Kopp, G., Heuerman, K., and Lawrence, G., "The Total Irradiance Monitor (TIM): Instrument Calibration," *Solar Physics*, 230, 1, Aug. 2005, pp. 111-127, doi:10.1007/s11207-005-7447-3
5. Kopp, G., Heuerman, K., Harber, D., and Drake, V., "The TSI Radiometer Facility - Absolute Calibrations for Total Solar Irradiance Instruments", Proc. SPIE 6677, 667709 (2007), doi:10.1117/12.734553
6. Kopp, G., "Solar Variability Magnitudes and Timescales," *Journal of Space Weather and Space Climate*, **6**, A30, 11 pp., 2016, doi:10.1051/swsc/2016025
7. Kopp, G., http://spot.colorado.edu/~koppg/TSI
8. Pankratz, C., Earth Observing System SOlar Radiation and Climate Experiment (EOS SORCE) Algorithm Theoretical Basis Document, Document No. 20560-T6-0006, 2000